Structural Monitoring of NiB_i Modified $BiVO_4$ Photoanodes Using in Situ Soft and Hard X-ray Absorption Spectroscopies

Lifei Xi,[†,] Martin Schellenberger,[†] Raphael Francesco Praeg,[†] Daowei Gao,[†,§] Dorian Drevon,[†] Paul Plate,[‡] Peter Bogdanoff,[‡] Roel van de Krol,[‡,*] and Kathrin M. Lange[†,¦,*]*

[†]Young Investigator Group Operando Characterization of Solar Fuel Materials (EE-NOC), [§]School of Chemistry and Chemical Engineering, University of Jinan, Jinan 250022, PR China [‡]Institute for Solar Fuels, §Institute Methods for Material Development, Helmholtz-Zentrum Berlin für Materialien und Energie GmbH, 12489 Berlin, Germany [¦] Universität Bielefeld, Physikalische Chemie, 33615 Bielefeld, Germany.

KEYWORDS. soft XAS, hard XAS, in situ, $BiVO_4$, nickel borate (NiB_i), photoanode

ABSTRACT. Photoelectrochemical (PEC) water splitting, a process using solar light and semiconductor to split water, is proposed as a potentially scalable method to store solar energy through renewable H_2 fuels. Obtaining the electronic structure information of co-catalyst is a crucial step towards gaining a mechanistic understanding of the water oxidation reaction of this catalyst. In the present work, we show that the PEC performance of $BiVO_4$ photoanodes can be enhanced by the deposition of a nickel-borate co-catalyst layer (NiB_i). We investigate the electronic structure of the NiB_i by in situ soft and hard X-ray absorption spectroscopies (XAS) at the Ni L- and K-edge as well as at the O K-edge under different potential and the illumination conditions. We discuss the involvement of the active oxygen species related to the hybridized O 2p-Ni $3dt_{2g}$ orbitals in the oxygen evolution reaction (OER) and further correlate the changes at the O *K*-edge with that of at the Ni L-edge. In situ soft XAS measurements show that Ni in

the electrodeposited amorphous NiB_i film is readily oxidized to higher oxidation states. This in situ soft XAS studies offer the first direct observation of Ni^{4+} formation during solar water oxidation. Cyclic voltammetry-XAS (CV-XAS) results support that the formation of Ni^{4+} is prior the formation of partly electron deficient oxygen sites. This study also proves that understanding the physical and chemical changes under potential and light illumination and represents a significant step toward obtaining a mechanistic understanding of the co-catalyst/semiconductor system.

INTRODUCTION

Photoelectrochemical (PEC) water splitting, a process using solar light and semiconductor to split water, is proposed as a possible scalable approach to store solar energy through H_2 fuels.[1,2] $BiVO_4$ is a promising photoanode material for the production of O_2 from water due to its suitable physical and chemical properties. [2,3] However, bare $BiVO_4$ films has poor electron transport, surface recombination,[4] and moderate catalytic activity. In recent years, modification of $BiVO_4$ photoanodes with co-catalysts, for example,CoO_x,[5] cobalt borate (CoB_i),[6] cobalt phosphate (CoP_i),[7,8] FeOOH,[9] FeOOH/NiOOH,[10] and manganese phosphate (MnO_x),[11] was found to be an effective method to enhance its photocatalytic performance.[5] Recently, nickel-borate (named as NiB_i) has been reported as another promising catalyst for oxygen evolution reaction (OER).[12] Cho et al. found that NiB_i successfully catalyzes the PEC water oxidation at 1.23 V_{RHE} when combined with a $BiVO_4$ photoanode.[13] Both electrodeposited and photodeposited NiB_i films improve the photocurrent of $BiVO_4$ at 1.23 V_{RHE} by 3-4 times under AM 1.5 illumination as well as *ca.* 250% enhancement in the photon-to-current efficiencies. Hilliard *et al*. attributed the increase of photocurrent at low potentials to NiB_i, which helps to withdraw charges at the semiconductor/electrolyte interface.[14] The catalytic performance of NiB_i should relate to their electronic structure.[15,16] The local electronic structure and OER mechanism of bare NiB_i catalyst films have been investigated using in situ soft XAS at the O

K-edge[15] and hard XAS at the Ni K-edge. [15,16] Still missing is an in situ electronic structural information of the Ni L-edge of NiB_i when coupled with a semiconductor. The electronic structure of NiB_i can change substantially when the NiB_i catalyst is deposited on a semiconductor [15] and tested under solar water oxidation conditions.

XAS is a powerful element-selective tool in studying electronic and crystal structure of catalyst. Soft XAS can provide the information of partially occupied transition metal 3d orbitals, O 2p orbitals, and the orbital hybridization.[17] It provides more detailed information than hard XAS because of the narrower natural line widths (Ni K-edge: 1.44 eV; Ni L-edge: 0.48 eV).[18] On the other hand, hard XAS can give complementary information on the oxidation states and the metal-ligand distances as well as the coordination geometries.[17] The main aims of the current study are: (a) to unravel the electronic structure of NiB_i modified $BiVO_4$ photoanodes under the solar water oxidation condition, and (b) to understand the OER catalytic cycle and the formation of active sites. Obtaining this structural and reaction information of the co-catalyst can be a significant step to mechanistically understand the solar water oxidation process.

EXPERIMENTAL SECTION

Chemicals. Nickel(II) nitrate hexahydrate ($Ni(NO_3)_2 \cdot 6H_2O$, 99.999% trace metals basis), boric acid (H_3BO_3, 99.5%), NaOH (>98%), NiO, $LiNiO_2$ and potassium nickel (4+) paraperiodate (NiPPI) were ordered from Sigma-Aldrich. More detailed information about the preparation of the borate buffer solution, the preparation of $BiVO_4$ film and the suppliers of the Si_3N_4 membranes as well as FTO glass substrates can be found in previous work.[11,19,20]

Electrodeposition of NiB_i. The details of our electrochemical setups can be found in our earlier papers.[11,21,22] All potentials reported in this paper are converted to the RHE scale. For electrodeposition, a freshly prepared nitrogen purged B_i buffer solution (0.2 M) containing 0.5 mM Ni^{2+} is used. For XAS measurements of NiB_i on a $BiVO_4$ photoanode, electrodeposition is performed at 1.85 V for 10-20 min without stirring and without iR compensation. The thickness

of NiB_i is around 100 nm. We find that for the $BiVO_4$/FTO substrate the maximum photocurrent density is usually obtained for an electrodeposition duration of 2-5 min. For comparison, NiB_i is also potentiostatically deposited on FTO/glass or Au/Si_3N_4 substrates at 1.85 V from a 0.2 M B_i electrolyte containing 0.5 mM Ni^{2+}. After the electrodeposition, all samples are rinsed with DI water.

Characterization. (a) Experimental details for the characterization of the morphology, chemical composition, crystal structure, photoelectrochemical (PEC) properties, and differential electrochemical mass spectroscopy (DEMS) can be found in previous works.[11,21,22] The electrolyte is 0.2 M B_i buffer solution (pH 9.2). The scan rate for LSV is 25 mV s^{-1} while that for DEMS is 5 mV s^{-1}. For DEMS experiments, the light intensity was adjusted to 1.5 suns in the range of 400nm to 900nm. (b) In situ soft XAS characterization: detailed information on the experimental conditions for the in situ XA measurements can be found in our previous papers[11,21,22]. Here, one white LED is used to illuminate the $BiVO_4$ photoanode. The energy resolution of the beamline is 208 meV at 850 eV. The experimental spectra are baseline-subtracted, normalized by the integrated area under the whole L-edge region, and then fitted with linear combination fitting using the experimental spectra of NiO, $LiNiO_2$ and NiPPI. The spectra of the Ni reference powders are carried out in a total electron yield (TEY) mode. Energy calibration of Ni L-edge spectra was carried out with the 852.00 eV peak using the NiO powder spectrum. Energy calibration of O K-edge spectra was done using the pre-edge feature of water at 535 eV and then normalized using the intensity at 548 eV. To obtain the spectrum for Ni^{4+} species, we subtract the Ni^{2+} spectrum from that of NiPPI as recently reported.[23] (c) In situ hard XAS characterization: the details can be found in our previous works.[19] The energy calibration is done using a nickel foil. For comparison, several Ni oxides or compound powders are measured as references.

RESULTS AND DISCUSSION

1. Surface Morphology, Phase, Composition, and Photoelectrochemical (PEC) Analysis.

Figures 1 and S1 show SEM images of the bare and modified $BiVO_4$/FTO photoanodes. It can be seen that the morphology changes after NiB_i modification. The surface of the $BiVO_4$ photoanode is nearly fully covered by a NiB_i amorphous layer, which leads to charging effects during the SEM measurements (see Figure 1b and c). The X-ray diffraction (XRD) patterns of the NiB_i modified $BiVO_4$, bare $BiVO_4$, and NiB_i/FTO films are shown in Figure S2a. The XRD pattern of the NiB_i-modified $BiVO_4$ is nearly identical as that of bare $BiVO_4$, while that of bare NiB_i is nearly identical to that of the FTO/glass substrate. Previous EXAFS results show that the NiB_i film contains sheets/disks composed of edge shared NiO_6 octahedra with domain sizes of 2-3 nm in diameter. [16] Such small domain crystallites are indeed difficult to detect by XRD since they appear as very broad peaks. The XRD pattern of the $BiVO_4$ film does not show significant changes after deposition of the NiB_i. Energy-dispersive X-ray spectroscopy (EDS) results clearly show the presence of Ni, Na and boron (B) in the film which confirms the successful NiB_i deposition (see Figure S2b). Figure 2 shows the PEC performance of the bare and the NiB_i-modified $BiVO_4$/FTO photoanodes. It can be seen that the photocurrent density of the $BiVO_4$ photoanode with NiB_i modification reaches 0.76 mA cm^{-2} at 1.23 V compared to 0.64 mA cm^{-2} for the bare $BiVO_4$, equivalent to a 19 % improvement. The photocurrent onset potential (V_{onset}) of the NiB_i modified photoanode shows a clear cathodic shift compared to the bare $BiVO_4$ photoanode under illumination, to a value of*ca.* 0.3 V vs. RHE. The enhancement of the photocurrent is especially pronounced at modest applied bias potentials (0.3 - 0.75 V). According to Peter's theoretical considerations,[24] this behaviour indicates either a reduction of surface recombination (i.e., passivation) by NiB_i or an increased catalytic activity of the film. Furthermore, the dark current of the NiB_i modified $BiVO_4$/FTO photoanodes is clearly cathodically shifted due to the redox charging of co-catalyst layer. This could be due to the fact that a certain amount of NiB_i may also have been deposited directly on exposed FTO. Possible reasons for the photocurrent enhancement and the V_{onset} shift are probably due to the increasing

catalytic activity and/or surface passivation. [19] However, Laskowski et al. very recently employed in situ atomic force microscopy (AFM) to track the flow of photogenerated holes in co-catalyst modified semiconductor.[25,26] They proposed that the co-catalyst layer collect photogenerated holes from the semiconductors (Si, Fe_2O_3 or $BiVO_4$), charging to potentials high enough to drive the OER. The co-catalyst layer, $Ni(Fe)O_xH_y$ or CoO_xH_y, is proposed to create charge-separating heterojunctions with the semiconductor and serve as OER catalysts.[25,26] Thus, a redox charging effect may also contribute to the V_{onset} shift. It is worth mentioning that the V_{onset} is located at a significantly more positive potential than the flatband potential (V_{fb}) reported for $BiVO_4$. This is most likely due to some remaining surface recombination, i.e., incomplete passivation of the $BiVO_4$ surface by NiB_i. Differential electrochemical mass spectrometry (DEMS, see Figure S3) measurements show that after NiB_i deposition, the amount of oxygen gas that evolves from the NiB_i modified $BiVO_4$ photoanode is greatly enhanced as evidenced by the photocurrent and O_2 gas evolution signals, indicating an increased Faraday efficiency.

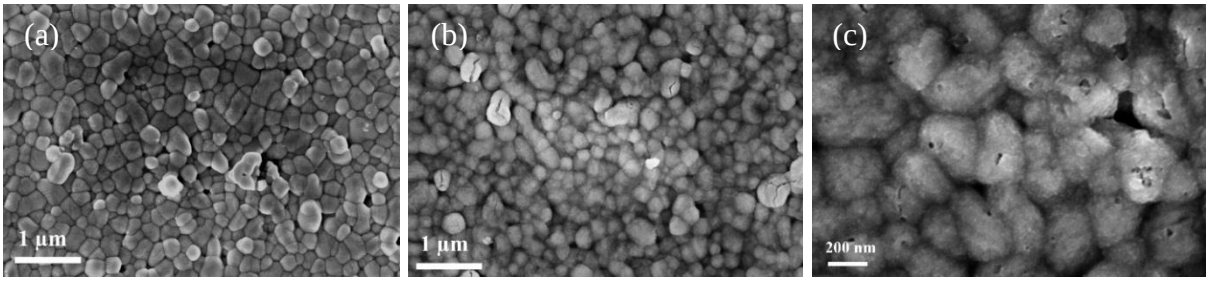

Figure 1. SEM images of the $BiVO_4$ photoanode: (a) before and (b-c) after deposition of NiB_i.

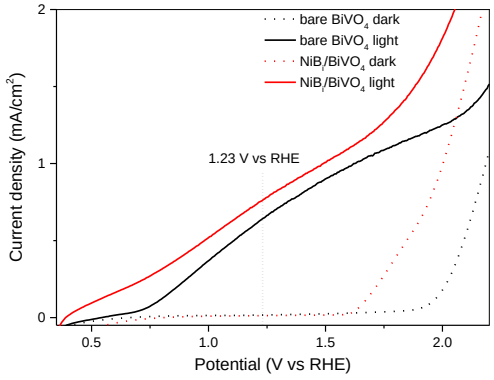

Figure 2. Linear sweep voltammetry (LSV) profiles of the bare and NiB_i modified $BiVO_4$/FTO photoanodes tested in the dark (dotted lines) and under illumination (solid lines). The scan rate was 25 mV s^{-1}. The light intensity was adjusted to 1.5 sun in the range of 400nm to 900nm.

2. In Situ XAS Analysis at the Ni L and K-edges.

2.1 In situ soft XAS at the Ni L-edge. Figure 3 shows in situ soft XAS results of the NiB_i modified $BiVO_4$/Au/Si_3N_4 photoanode under different potentials and illumination conditions. The electrolyte is a 0.2 M B_i buffer solution with 2.0 M KNO_3 added. It is worth mentioning that the light intensity for all in situ XAS tests are significantly lower than that of above mentioned LSV due to the weak light source (a white-LED used) and the absorption of Si_3N_4 membrane window. For a detailed analysis of the sample, nickel oxide reference spectra of NiO (2+), $LiNiO_2$ (3+) and potassium nickel (4+) paraperiodate (named as NiPPI) are also tested and shown at the bottom panel of Figure 3a. The Ni L-edge XA spectra of the reference powders and the samples contain two characteristic broad multiplet peaks: L_3 and L_2. They are separated by ~ 17 eV due to the core-hole spin-orbit interaction. The fine splittings of both L_3 and L_2 arise from O 2p-Ni 3d interactions and the crystal field effect from the local ligand coordination environment. [23, 27,28] It can be observed from Figure 3a that as the oxidation state increases from Ni^{2+}, Ni^{3+} to Ni^{4+}, the Ni L_2-edge resonance intensity of the reference spectra also increases because of the increased number of holes in the d-states (see Table S1 and S2). In all these reference powders the Ni is octahedrally coordinated.[29,30] In an octahedral symmetry, the Ni 3d band separates into three lower energy orbitals (t_{2g}: d_{xy}, d_{xz} and d_{yz}) and two higher energy orbitals (e_g: $d_{x^2-y^2}$ and d_{z^2}) (see Table S2). The crystal field splitting and the energy position of the L-edge spectrum are affected by the number of unpaired 3d electrons which defines the oxidation state.

In Figure 3a, pronounced spectral changes upon varying potential and illumination conditions of the sample are observed for both the L_3- and L_2-edges. The dashed vertical lines indicate the peaks at which major changes occur. The energetic peak positions and the relative intensity

ratio of the double-peak features are closely associated with the relative amounts of Ni in different oxidation states. We assign the Ni L_3 spectral features at 852.00 and 854.45 eV to contributions of the Ni^{2+} and Ni^{4+} species, respectively. The chemical shift of 2.45 eV between Ni^{2+} and Ni^{4+} matches the reported value. [23] The data show that Ni species gradually oxidize from 2+ to 4+ at potentials positive of 1.75 V. In the Ni L_2-edge, a growing L_2-edge signal around 871.4 eV confirms the generation of Ni^{4+} species, as proposed recently. [23]

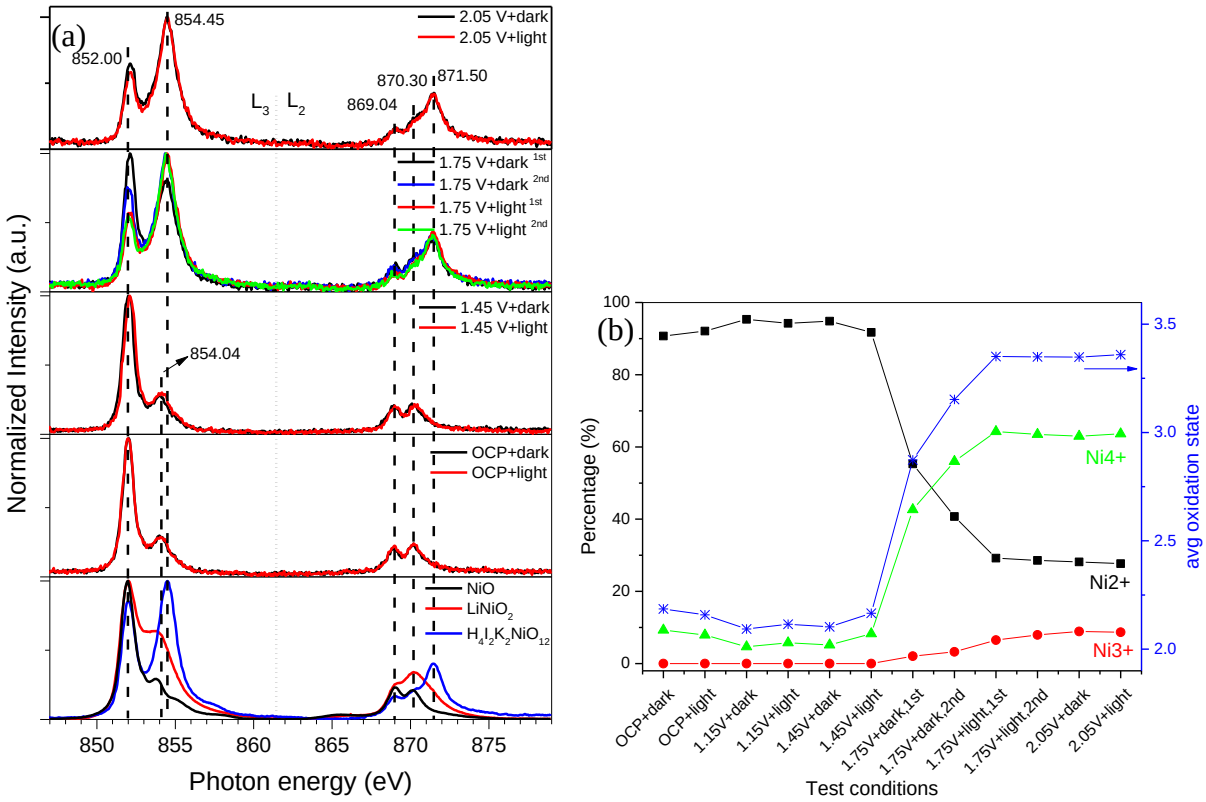

Figure 3. (a) In situ Ni L-edge spectra of a $NiB_i/BiVO_4/Au/Si_3N_4$ photoanode measured under different conditions. The test sequence is OCP, 1.15 (not shown), 1.45, 1.75 and 2.05 V, first in the dark and then under illumination (with one white LED). (b) Relative contributions of the different Ni oxidation states obtained from linear combination fitting of the XAS data. The test sequence is the same as mentioned as Figure 3a.

Figure 3b presents the fitting results for the tested Ni L-edge spectra (see Figure S4 for an example of the fitted spectra). The as-prepared NiB_i modified $BiVO_4$ photoanode at OCP and under dark conditions contains ~90 % of Ni^{2+} and ~10 % of Ni^{4+}. This corresponds to an average oxidation state of ~2.19, implying that the as-prepared NiB_i modified $BiVO_4$ photoanode is dominated by Ni^{2+}. No effect of visible light illumination on the spectrum was observed at OCP

or at 1.15 V. This behavior differs from our previous observation on MnP_i modified $BiVO_4$ photoanodes, [11] where even at OCP and under illumination conditions, Mn species in the MnP_i film were found to be gradually oxidized by the photopotential or photobias. The photopotential is very recently found as big as 0.9 V.[25,26] This means that NiB_i or MnP_i modified $BiVO_4$ photoanodes differ in their electronic structure, specifically in their charge transfer properties.

When changing the potential from OCP to 1.15 V, and further to 1.45 V under dark conditions, it is found that the average oxidation state of Ni slightly decreases from 2.19 to 2.10. The observed oxidation state decrease can be due to a slow catalyst relaxation and/or beam damage. At 1.45 V and under illumination, an oxidation process of Ni occurs. In the Ni L_3-edge spectra, for instance, a small shoulder at around 854.50 eV is intensified which is absent in the dark. This means that under a moderate band bending the photo-generated holes in $BiVO_4$ are transferred and oxidize the NiB_i film. Under illumination, the applied potential and the photopotential provided by the semiconductor make the water oxidation feasible. This is indeed supported by the evolution of the peak at 531.30 eV at the O K-edge which will be discussed later in the Section 3. The linear combination fitting results show that there are 92% Ni^{2+} and 8% Ni^{4+} in the film. This corresponds to an average oxidation state of 2.17, which is nearly identical to the value of 2.19 obtained under OCP. At 1.75 V in the dark (during the 1st scan), the film is rapidly oxidized which is evidenced by the fast spectral changes from the 1st to the 5th scan (see also Figure S5a for the time-dependent XA spectra). For example, the intensity of the peak at 852.0 eV gradually decreases while that at 854.45 eV simultaneously increases. Accordingly, the percentage of Ni in the film significantly varies. After the 1st scan, there are 55% Ni^{2+}, 2% Ni^{3+} and 43% Ni^{4+} species corresponding to an average oxidation state of 2.87 while after the 2nd and 5th scans, the average oxidation states increase to 3.15 and 3.31, respectively. This prominent oxidation state change reflects a significant change in both the electronic and crystal structure of the NiB_i film. When the light is switched on at this potential, the film is slightly further oxidized to an average oxidation state of 3.35. At such positive

potentials (far above OER), there is significant band bending in the $BiVO_4$ and the photogenerated holes are efficiently transferred to the Ni sites where they oxidize NiB_i. At 2.05 V in the dark or under illumination, the film is continuously oxidized as seen from the decreasing peak intensity at 852.0 eV. The percentage of Ni^{4+} species in the film increases. When comparing the trace of the Ni L-edge spectrum at +2.05 V under illumination with that of subtracted NiPPI (see Figure S5b), the Ni L-edge spectrum in the electrodeposited $NiB_i/BiVO_4$ photoanode approaches that of NiPPI. But the peak intensity at 852.15 eV is still lower (see the dashed line), meaning that a portion of the Ni ions stays in the lower oxidation state. The average oxidation state is 3.36. A moderately high oxidation state of the NiB_i catalyst film was previously proposed to lead to a higher OER activity. [16] Overall, our in situ soft XAS studies show that Ni in the electrodeposited amorphous NiB_i film is readily oxidized to high oxidation states. Moreover, our studies offer the first direct observation of Ni^{4+} formation during solar water oxidation.

2.2 In situ hard XAS at the Ni K-edge. The X-ray absorption near edge structure (XANES) transition metal K-edge spectra are dominated by transitions from core 1s → np final states (the dipolar transitions, the lowest unoccupied states). [17, 29] They give detailed information about the oxidation state as well as coordination geometries of the metal atoms. The extended X-ray absorption fine structure (EXAFS) spectra are dominated by the scattering of photoelectrons ejected from the absorbing atom by the photo-electric effect. They provide information on the local environment of the atom, for example, the number and type of ligands and their distances to the central atom. [17] For an amorphous metal oxide catalyst film where X-ray diffraction techniques are not suitable (since they depend on long-range order), the ability to probe the local structure of these films is a major advantage of XAS. [29] In this study, in situ hard XAS spectra recorded in fluorescence mode are performed (see Figure 4). Similar to the soft XAS measurements, the spectra of NiO, $LiNiO_2$, and NiPPI powders are also collected (see the lower panel in Figure 4). It is found that there is nearly no shift of the Ni K-edge when changing the

potential from OCP to 1.45 V in the dark. At 1.75 V, the edge shift is around 4.2 eV. Further increasing the potential leads to a shift to higher energies. Under illumination, the edge shift is *ca.* 3.1 eV when switching the potential from 1.15 V to 1.45 V (see the top panel in Figure 4). Thus, upon moderate band bending the photo-generated holes in $BiVO_4$ oxidize the NiB_i film, which is consistent with the soft XAS results.

Figure S6a shows an overview of the observed Ni K-edge shifts for different oxidation states and for different applied potentials, both in the dark and under illumination. From the calibration curve obtained by a modified integral method, [27] we estimate an energy shift of around 2.15 eV per unit change in the nickel oxidation state. The integrated edge position of the NiB_i-modified $BiVO_4$ film at the OCP and in the dark is slightly higher than that of NiO (8347.63 eV). The average oxidation state is around +2.04. Whereas after oxidation at 1.75 V in the dark, the edge shape of the film changes and the edge position shifts to 8350.42 eV, corresponding to a maximum edge shift of +2.79 eV. The average Ni oxidation state is 3.36, indicating that the fraction of Ni with higher oxidation state increases. At 2.05 V in the dark, the film is further oxidized and the average oxidation state is around 3.48. When light is switched on and the potential is increased, the integrated edge position shifts faster to higher energies than under dark conditions. At 2.05 V, the integrated edge position approaches to that of NiPPI. The obtained trend of the oxidation process is in good agreement with our soft XAS results.

Figure S6b presents the Fourier transformed EXAFS spectra of the NiB_i modified $BiVO_4$ photoanode tested at OCP and at 2.05 V. In these spectra, the peak positions reflect the average bond distances between neighboring atom pairs while the amplitude of the peaks can be a rough indicator of the number ofneighboring atoms. [29] It is found that the bond distance change for Ni-O and Ni-Ni under different potential and illumination is nonequivalent. This is attributed to the relaxation of the Jahn-Teller distortion. [15,16] This results in formation of nanoscale ordered NiO_6 octahedra domains in the NiB_i electrocatalyst. [15] Bediako et al. proposed that this relates

to the transformation from inactive NiB_i with a β-NiOOH structure (Ni^{3+}) to active NiB_i containing a γ-NiOOH structure ($Ni^{3.6+}$).[16] The intensities of the peak correlating to a Ni-Ni distance of 2.05 Å are higher than the ones at the OCP in the dark, indicating a more extended long range order in the NiB_i film.

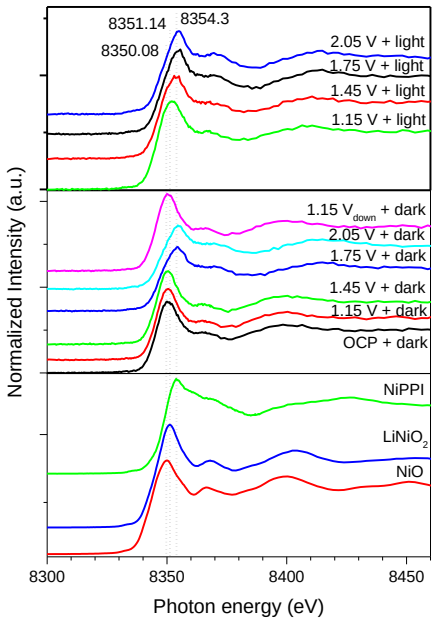

Figure 4. In situ Ni K-edge spectra of a $NiB_i/BiVO_4$/FTO photoanode measured at different potentials and under illumination conditions. The test sequence for dark and light condition, respectively, is: OCP, 1.15 V, 1.45 V, 1.75 V and 2.05 V. The reference oxide spectra are NiO, $LiNiO_2$ and NiPPI. The spectra are baseline subtracted and intensity normalized at 8460 eV.

3. In Situ Soft XAS Analysis at the O K-edge.

Investigations using in situ soft XAS at the O K-edge of NiB_i modified $BiVO_4$ can provide valuable information on the interaction as well as the degree of orbital hybridization between the transition metal 3d and the O 2p states. [15, 17, 28,31] O K-edge spectra of the $BiVO_4$ photoanodes under different potentials and illumination conditions are presented in Figure 5. Reference spectra of the O K-edge from liquid water, water vapor, O_2 gas [32], NiO, $LiNiO_2$, NiPPI, and V_2O_5 are also presented for comparison (see Figure S7a). After subtracting a baseline, all O K-edge spectra are normalized to the intensity at 548 eV. In the upper panel of Figure 5, the O K-edge spectra can be split into three distinct regions.[33] The high energy region (> 538 eV) corresponds to the EXAFS region relating to the excitation of O 1s to O 2p, O 1s to

metal states (4sp for V and Ni or 6s6p mixed states for Bi[34]), and the O 1s → σ* transition in both liquid water and water vapor [15, 32] present in the X-ray path. The intermediate energy region (534 - 538 eV) is assigned to near edge transitions of the water molecule. [32] For example, the peaks at 534.23 and 534.69 eV relate to water vapor while the peak at 535.54 eV relates to the liquid water pre-edge. A zoom-in of the low energy region (527.5 - 534 eV) is presented in the lower panel of Figure 5. The features in this region have been previously assigned to the electronic transitions from the O1s shell to the hybridized states of O 2p with Ni 3d 2p orbitals.[35] Using Gaussian multi-peak fitting, several distinct contributions can be distinguished (see Figure S7b and Table S3-4). The peak at 529.17 eV appears at potentials from 1.45 V and above, i.e., at pre-catalytic potentials (under dark condition) before the O-O bond formation, [33] for the NiB_i modified $BiVO_4$ film. This peak will be discussed in detail later. Similarly, the feature at 530.16 eV increases slightly at higher potentials and is assigned to transitions from the O1s to O 2p orbitals mixed with V 3d based on our V_2O_5 reference spectrum (see Figure S7a). The peak at 531.30 eV slightly increases in intensity and is commonly assigned to the O 1s → O(π*) transition of O_2 gas, [15, 32] implying the evolution of oxygen gas at these potentials and under illumination. It is found that at 2.05 V this peak intensity is increased 1.74 times compared to that at the OCP, implying O_2 gas evolution at the electrode. The peak at 533.96 eV is assigned to the orbital hybridization of O2p with Ni-OH. [15]

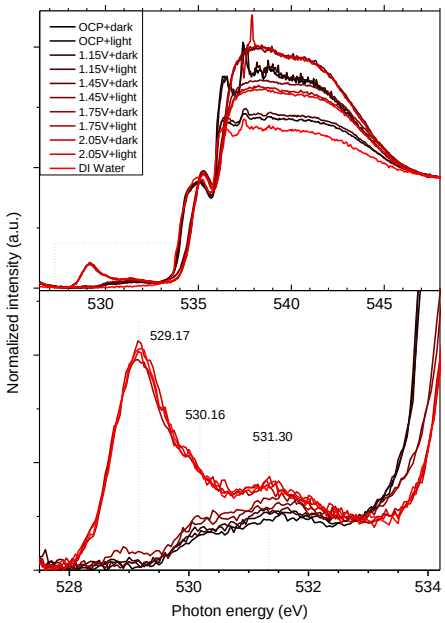

Figure 5. In situ XAS O K-edge spectra of a $NiB_i/BiVO_4/Au/Si_3N_4$ photoanode tested under different conditions. The test sequence is OCP, 1.15 V, 1.45 V, 1.75 V and 2.05 V, first in the dark and then under illumination. The spectra are baseline-subtracted and then intensity-normalized at 548 eV.

In the following the intensity changes of the peaks at 529.15 eV will be discussed, which is of high relevance for this study. The origin of the spectral changes under applied potential is proposed as below: we know that the O K-edge and Ni L-edge data reflects different electronic structure information. In the Ni L-edge spectrum, X-ray absorption is caused by the excitation of a Ni 2p electron to unfilled 3d orbitals which creates the characteristic absorption peaks. [17, 28] The shift of Ni L-edge position is because of the changing number of unpaired 3d electrons. The O K-edge spectrum is sensitive to the metal atom coordination geometry and the unoccupied p-weighted density of states (pDOS) following the dipole selection rule. [34, 35,36] In NiB_i, O 2p states hybridize with Ni 3d orbitals and thus the lowest energy fine structure is governed by the ligand-to-metal charge transfer excitations. The appearance of the peak at 529.17 eV under high potential reflects the increase in oxidation state of Ni and corresponds to transition from O 1s orbitals to hybridized - O 2p-Ni $3d_{t2g}$ orbitals (in an octahedral field). At high external potentials, electrons are removed from Ni ions via a structural transformation process (deprotonation) and Ni^{2+} is oxidized to Ni^{4+}.[16] Based on our XAS results, the as

prepared NiB_i film contains 91 % Ni^{2+} and 9% Ni^{4+} species at the resting state, thus mostly contains a big portion of surface and defects Ni^{2+} sites. These sites are probably readily oxidized under external potential. Contrary to the pristine $Ni^{2+}(3d^8)$ state (see Table S2), which lies above the O 2p orbitals, the newly evacuated Ni 3d states (Ni^{3+} ($3d^7$) and Ni^{4+} ($3d^6$)) hybridize with the O 2p band and shift to a deeper binding energy below the O 2p orbitals.[37] Consequently this pushes the O 2p level up to a higher energy, which thus gets closer to the Fermi level. The smaller binding energy required for partial transfer of O electrons to Ni 2p hole significantly facilitates a ligand-to-metal charge transfer (LMCT). The formation of a high valence Ni^{4+} site makes the bound O species electrophilic and transforms them into oxo or oxyl radical species.[38,39] These oxo or oxyl groups are susceptible to nucleophilic attack by water molecules which then coordinate as terminal ligands to Ni^{4+}, which is the most critical step before bimolecular oxygen gas release. The concentration of O 2p holes, whose presence manifests as the O K-edge pre-edge feature, can be an indicator of the active oxygen species formation. [33] The formation of the Ni^{4+} ions allows to activate these oxygen ions. [38] An alternative mechanism correlates to the oxyl radicals which format the Ni^{4+} site and which pair with a nearby Ni-bridging oxo group.[40] The Ni^{4+} mechanism proposed by us differs from the mechanism proposed in a previous study. [15] In that study, Yoshida et al. correlated the changes at 528.7 eV in the O K-edge spectra with the nanoscale ordered domain formationin the NiB_i electrocatalyst.

4. In Situ CV-XAS Test at Ni L-edge and O K-edge.

In order to dynamically monitor the changes shown in the Ni L- and O K-edges, the XA transmission signal from the NiB_i-modified $BiVO_4$ photoanode is monitored during CV cycling (see Figure 6). The incoming photon energy is fixed at either 529.15, 852.05 or 854.25 eV for the O K-edge or Ni *L*-edge feature because the absorption at these peaks is observed to vary when changing the external potential and illumination conditions. As mentioned above, the absorption at 529.15 eV relates to the hybridized O 2p-Ni $3dt_{2g}$ orbitals and acts as an indicator of the formation of active oxygen species. The absorption at photon energies of 852.05 or

854.25 eV at Ni L_3-edge reflects the oxidation or reduction of nickel in the NiB_i film, respectively. During the CV cycling under dark and light conditions, the absorption at both energies of 529.17 eV and 854.25 eV (relating to Ni^{4+} species) follows a similar behavior (see Figure 6). Both absorption traces start to rise at potentials above 1.50 V, which is at pre-catalytic potentials under dark condition. [33] All traces, either under illumination or in the dark, steadily grow during the anodic scan but with a different rate while entering the OER region under the effect of photopotential. The relatively fast rise of the traces related to Ni^{4+} species (red and blue curves in Fig. 6) further supports that the formation of the Ni^{4+} ions allows to activate these oxygen ions. It can also imply that the formation of active O species is a relatively slow process. The traces continue to grow until the potential scan reaches back to the onset of the reduction wave (1.50 V). When decreasing the potential below 1.5 V, the intensities of the 854.25 and 529.17 eV signals rapidly decay back to nearly the initial levels, albeit with different rates. It is found that the intensity at 854.25 eV (Ni^{4+}) decays faster than that of O K-edge pre-edge feature. This further proves that the O K-edge and Ni L-edge reflect different electronic structure information of the film. For the intensity at 529.17 eV, the fast decay finishes at 0.94 V and 0.84 V under dark and light conditions, respectively. There is a 100 mV delay, corresponding to 10 s testing time. For the absorption at 854.25 eV, the fast decay ends at 1.0 V and 0.96 V under dark and light conditions, respectively, corresponding to 40 mV delay or 4 s testing time. The reason for the slight delay of decay when the light is on is due to the oxidation effect of photo-induced holes. Toward the end of the CV scan, two signals nearly decay back to the initial levels. This means that Ni returns to its low oxidation state and implies a reversible redox nature of Ni^{4+}/Ni^{2+}. This is not visible in steady state XAS measurements and further illustrates the advantage of the CV-XAS technique.

The absorption at 852.05 eV (Ni L-edge relating to Ni^{2+} species) nicely tracks the CV cycling behavior in the dark. On the anodic sweep from 0.55 V to 1.75 V, the trace increases slightly which means that reduction occurs, probably due to the catalyst relaxation or beam damage. At

potentials positive of 1.75 V (i.e., well within the OER region), the trace decays fast, even during the reverse scan, implying a fast oxidation process of Ni species. The trace decays slowly until a potential of 1.10 V. This so-called hysteresis phenomenon, meaning that the reduction is more difficult than the oxidation, was observed previously.[15, 33] The trace starts to increase till the end of the scan corresponding to the recovery of Ni^{2+} species in the film.

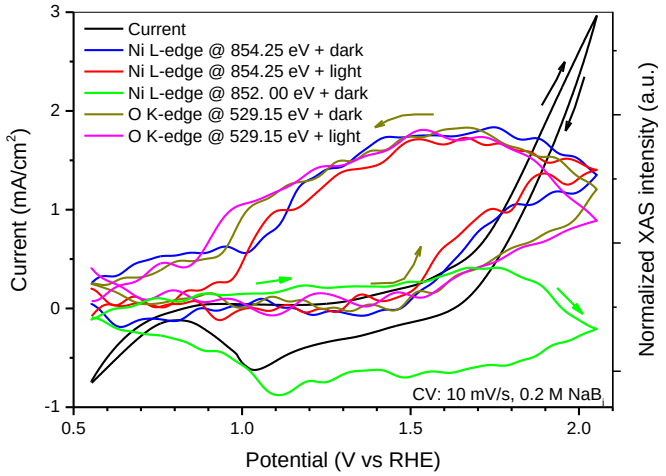

Figure 6. In situ CV-XAS results of a $NiB_i/BiVO_4/Au/Si_3N_4$ photoanode. The CV curve showed is measured under dark while the X-ray transmitted signals are tested under different photon energies and light conditions.

5. The Mechanism

Based on the results described above, we propose the mechanism described in Figure 7 for water oxidation at NiB_i in contact with a $BiVO_4$ photoanode. The pre-catalytic state is defined as the potential being below 1.45 V_{RHE} under dark condition. We knew that under light condition, the pre-catalytic state should be even lower due to the photopoential. Above this potential Ni^{2+} species are rapidly oxidized to Ni^{4+}. In this study, we did not observe the stepwise Ni oxidation that we recently reported for the $FeNiO_x$ system.[33] The amount of Ni^{3+} is negligible in these NiB_i films. A possible reason is that this state is too short-lived to observe with steady state XAS in this highly active co-catalyst. Our CV-XAS results further support the fast transition of Ni species. Maintaining a potential positive of 1.75 V results in charge redistribution from O 2p to Ni 3d as proposed previously.[33] This will lower the average Ni oxidation state through formation of $Ni^{+4-\delta}$ and a concomitant increase of the oxygen oxidation

state through the formation of $O^{-2+\delta}$. From the CV-XAS as well as the steady state O K-edge results, we propose that the formation of electron deficient oxygen sites is strongly correlated to the Ni oxidation step, resulting in a stable precursor state prior to the O-O bond formation.[33] The $Ni^{+4-\delta}$-$O^{-2+\delta}OH$ species are further oxidized to a $Ni^{+4-\delta}$-$O^{-2+\delta}O$ species which subsequently release water and O_2 gas. After the OER, the dominant Ni^{4+} species are reduced to Ni^{2+} and the overall average oxidation state of film decreases. In recent years, it is found that the intentional or unintentional incorporation of Fe into Ni-layer double hydroxide (LDH) structures dramatically enhances OER activity.[25,41,42] The enhanced catalytic behavior has been attributed to the Lewis acidity of Fe (III), layered structures of LDHs, increased film conductivity, specific Fe incorporation sites at the edge and defects, and modulating the oxidizing capability of nickel and acting as the only active site.[43] Since there is no purification process for the electrolyte used and the trace level of Fe impurity is not "visible" and reflected on the XA spectrum, we cannot exclude the possibility of a small amount of Fe incorporating and thus affect the OER pathway as well as the proposed mechanism.

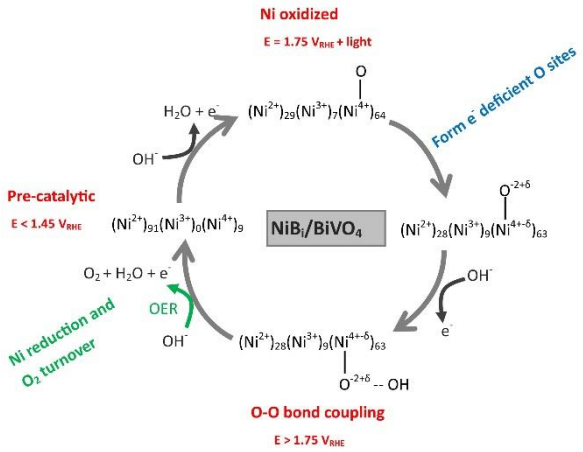

Figure 7. Schematic showing the NiB_i co-catalyst change observed in situ XAS measurements of the NiB_i modified $BiVO_4$.

CONCLUSION

In summary, we demonstrate that electrodeposited NiB_i enhances the PEC performance of a $BiVO_4$ photoanode. In situ soft and hard X-ray absorption spectroscopies are employed to get

the electronic structure information. We show that the Ni in the electrodeposited amorphous NiB_i film is in the 2+ state and is readily oxidized to higher oxidation states, even up to the 4+ state. This is the first time that the Ni^{4+} species are directly observed during light-driven water oxidation. We find that the oxidation of Ni is accompanied by an O K-edge pre-peak at 529.17 eV. We further discuss the involvement of the active oxygen species related to the hybridized O 2p-Ni $3dt_{2g}$ orbitals in the OER and further correlate the changes at the O *K*-edge with that of at the Ni L-edge. The formation of Ni^{4+} results in the formation of electron deficient oxygen sites. These sites act as electrophilic centers that lead to the formation of a stable precursor state prior to O-O bond formation. CV-XAS results support above argument and it is found that the hard XAS results are in good agreement with our soft XAS results.

ASSOCIATED CONTENT

SUPPORTING INFORMATION

The Supporting Information is available free of charge on the ACS Publications website at DOI:

Additional experimental, SEM images, EDS results, XRD patterns, XAS spectra, DEMS curves, linear combination fitting spectra, and tables (the peak position, the electronic configuration of Ni and O K-edge fitting results) (PDF).

AUTHOR INFORMATION

Corresponding Author

lifei.xi@helmholtz-berlin.de; roel.vandekrol@helmholtz-berlin.de; kathrin.lange@helmholtz-berlin.de

Notes

The authors declare no competing financial interest.

ACKNOWLEDGMENTS

The authors would like to thank I. Rudolph for the Au coatings and K. Harbauer for the assistance in the sample preparation. The authors also thank Drs. R. Golnak and G. Schuck for their support during the beamtime. This work was funded by the Helmholtz Association (VH-NG-1140).

REFERENCES

(1) Walter, M. G.; Warren, E. L.; McKone, J. R.; Boettcher, S. W.; Mi, Q.; Santori, E. A.; Lewis, N. S. Solar Water Splitting Cells. *Chem. Rev.* **2010**, *110* (11), 6446–6473. https://doi.org/10.1021/cr1002326.

(2) Sivula, K.; Le Formal, F.; Grätzel, M. Solar Water Splitting: Progress Using Hematite (α-Fe2O3) Photoelectrodes. *ChemSusChem* **2011**, *4* (4), 432–449. https://doi.org/10.1002/cssc.201000416.

(3) Trześniewski, B. J.; Smith, W. A. Photocharged BiVO4 Photoanodes for Improved Solar Water Splitting. *J. Mater. Chem. A* **2016**, *4* (8), 2919–2926. https://doi.org/10.1039/C5TA04716A.

(4) Zachäus, C.; Abdi, F. F.; Peter, L. M.; van de Krol, R. Photocurrent of BiVO4 Is Limited by Surface Recombination, Not Surface Catalysis. *Chem. Sci.* **2017**, *8* (5), 3712–3719. https://doi.org/10.1039/C7SC00363C.

(5) Jia, Q.; Iwashina, K.; Kudo, A. Facile Fabrication of an Efficient BiVO4 Thin Film Electrode for Water Splitting under Visible Light Irradiation. *Proc. Natl. Acad. Sci.* **2012**, *109* (29), 11564 LP-11569.

(6) Ding, C.; Shi, J.; Wang, D.; Wang, Z.; Wang, N.; Liu, G.; Xiong, F.; Li, C. Visible Light Driven Overall Water Splitting Using Cocatalyst/BiVO4 Photoanode with Minimized Bias. *Phys. Chem. Chem. Phys.* **2013**, *15* (13), 4589–4595. https://doi.org/10.1039/C3CP50295C.

(7) Pilli, S. K.; Furtak, T. E.; Brown, L. D.; Deutsch, T. G.; Turner, J. A.; Herring, A. M. Cobalt-Phosphate (Co-Pi) Catalyst Modified Mo-Doped BiVO4 Photoelectrodes for Solar Water Oxidation. *Energy Environ. Sci.* **2011**, *4* (12), 5028–5034. https://doi.org/10.1039/C1EE02444B.

(8) Jeon, T. H.; Choi, W.; Park, H. Cobalt–phosphate Complexes Catalyze the Photoelectrochemical Water Oxidation of BiVO4 Electrodes. *Phys. Chem. Chem. Phys.* **2011**, *13* (48), 21392–21401. https://doi.org/10.1039/C1CP23135A.

(9) Seabold, J. A.; Choi, K.-S. Efficient and Stable Photo-Oxidation of Water by a Bismuth Vanadate Photoanode Coupled with an Iron Oxyhydroxide Oxygen Evolution Catalyst. *J. Am. Chem. Soc.* **2012**, *134* (4), 2186–2192. https://doi.org/10.1021/ja209001d.

(10) Kim, T. W.; Choi, K.-S. Nanoporous BiVO4 Photoanodes with Dual-Layer Oxygen Evolution Catalysts for Solar Water Splitting. *Science (80-.).* **2014**, *343* (6174), 990 LP-994.

(11) Xi, L.; Wang, F.; Schwanke, C.; Abdi, F. F.; Golnak, R.; Fiechter, S.; Ellmer, K.; van de Krol, R.; Lange, K. M. In Situ Structural Study of MnPi-Modified BiVO4 Photoanodes by Soft X-Ray Absorption Spectroscopy. *J. Phys. Chem. C* **2017**, *121* (36), 19668–19676. https://doi.org/10.1021/acs.jpcc.7b06459.

(12) Dincă, M.; Surendranath, Y.; Nocera, D. G. Nickel-Borate Oxygen-Evolving Catalyst That Functions under Benign Conditions. *Proc. Natl. Acad. Sci.* **2010**, *107* (23), 10337 LP-10341. https://doi.org/10.1073/pnas.1001859107.

(13) Choi, S. K.; Choi, W.; Park, H. Solar Water Oxidation Using Nickel-Borate Coupled BiVO4 Photoelectrodes. *Phys. Chem. Chem. Phys.* **2013**, *15* (17), 6499–6507. https://doi.org/10.1039/C3CP00073G.

(14) Hilliard, S. Water Splitting Photoelectrocatalysis: The Conception and Construction of a Photoelectrocatalytic Water Splitting Cell, Université Pierre et Marie Curie – Paris VI, 2016.

(15) Yoshida, M.; Mitsutomi, Y.; Mineo, T.; Nagasaka, M.; Yuzawa, H.; Kosugi, N.; Kondoh, H. Direct Observation of Active Nickel Oxide Cluster in Nickel − Borate Electrocatalyst.

(16) Bediako, D. K.; Lassalle-Kaiser, B.; Surendranath, Y.; Yano, J.; Yachandra, V. K.; Nocera, D. G. Structure–Activity Correlations in a Nickel–Borate Oxygen Evolution Catalyst. *J. Am. Chem. Soc.* **2012**, *134* (15), 6801–6809. https://doi.org/10.1021/ja301018q.

(17) Gu, W.; Wang, H.; Wang, K. Nickel L-Edge and K-Edge X-Ray Absorption Spectroscopy of Non-Innocent Ni[S2C2(CF3)2]2nseries (n = −2, −1, 0): Direct Probe of Nickel Fractional Oxidation State Changes. *J. Chem. Soc. Dalt. Trans.* **2014**, *43* (17), 6406–6413. https://doi.org/10.1039/c4dt00308j.

(18) Krause, M. O.; Oliver, J. H. Natural Widths of Atomic K and L Levels, Kα X-ray Lines and Several KLL Auger Lines. *J. Phys. Chem. Ref. Data* **1979**, *8* (2), 329–338. https://doi.org/10.1063/1.555595.

(19) Xi, L.; Schwanke, C.; Zhou, D.; Drevon, D.; van de Krol, R.; Lange, K. M. In Situ XAS Study of CoBi Modified Hematite Photoanodes. *Dalt. Trans.* **2017**, *46* (45), 15719–15726. https://doi.org/10.1039/C7DT02647A.

(20) Gong, H.; Freudenberg, N.; Nie, M.; van de Krol, R.; Ellmer, K. BiVO4 Photoanodes for Water Splitting with High Injection Efficiency, Deposited by Reactive Magnetron Co-Sputtering. *AIP Adv.* **2016**, *6* (4), 45108. https://doi.org/10.1063/1.4947121.
(21) Schwanke, C.; Xi, L.; Lange, K. M. A Soft XAS Transmission Cell for Operando Studies. *J. Synchrotron Radiat.* **2016**, *23* (6), 1390–1394. https://doi.org/10.1107/S1600577516014697.
(22) Xi, L.; Schwanke, C.; Xiao, J.; Abdi, F. F.; Zaharieva, I.; Lange, K. M. In Situ L-Edge XAS Study of a Manganese Oxide Water Oxidation Catalyst. *J. Phys. Chem. C* **2017**, *121* (22), 12003–12009. https://doi.org/10.1021/acs.jpcc.7b02331.
(23) Zheng, X.; Zhang, B.; De Luna, P.; Liang, Y.; Comin, R.; Voznyy, O.; Han, L.; García De Arquer, F. P.; Liu, M.; Dinh, C. T.; et al. Theory-Driven Design of High-Valence Metal Sites for Water Oxidation Confirmed Using in Situ Soft X-Ray Absorption. *Nat. Chem.* **2018**, *10* (2), 149–154. https://doi.org/10.1038/nchem.2886.
(24) Peter, L. M.; Li, J.; Peat, R. Surface Recombination at Semiconductor Electrodes: Part I. Transient and Steady-State Photocurrents. *J. Electroanal. Chem. Interfacial Electrochem.* **1984**, *165* (1–2), 29–40. https://doi.org/10.1016/S0022-0728(84)80084-4.
(25) Nellist, M. R.; Qiu, J.; Laskowski, F. A. L.; Toma, F. M.; Boettcher, S. W. Potential-Sensing Electrochemical AFM Shows CoPi as a Hole Collector and Oxygen Evolution Catalyst on BiVO4 Water-Splitting Photoanodes. *ACS Energy Lett.* **2018**, *3* (9), 2286–2291. https://doi.org/10.1021/acsenergylett.8b01150.
(26) Laskowski, F. A. L.; Nellist, M. R.; Qiu, J.; Boettcher, S. W. Metal Oxide/(Oxy)Hydroxide Overlayers as Hole Collectors and Oxygen-Evolution Catalysts on Water-Splitting Photoanodes. *J. Am. Chem. Soc.* **2019**, *141* (4), 1394–1405. https://doi.org/10.1021/jacs.8b09449.
(27) Dau, H.; Liebisch, P.; Haumann, M. X-Ray Absorption Spectroscopy to Analyze Nuclear Geometry and Electronic Structure of Biological Metal Centers-Potential and Questions Examined with Special Focus on the Tetra-Nuclear Manganese Complex of Oxygenic Photosynthesis. *Anal. Bioanal. Chem.* **2003**, *376* (5), 562–583. https://doi.org/10.1007/s00216-003-1982-2.
(28) Palina, N.; Wang, L.; Dash, S.; Yu, X.; Breese, M. B. H.; Wang, J.; Rusydi, A. Investigation of the Metal-Insulator Transition in NdNiO3films by Site-Selective X-Ray Absorption Spectroscopy. *Nanoscale* **2017**, *9* (18), 6094–6102. https://doi.org/10.1039/c7nr00742f.
(29) Risch, M.; Klingan, K.; Heidkamp, J.; Ehrenberg, D.; Chernev, P.; Zaharieva, I.; Dau, H. Nickel-Oxido Structure of a Water-Oxidizing Catalyst Film. *Chem. Commun.* **2011**, *47* (43), 11912–11914. https://doi.org/10.1039/C1CC15072C.
(30) Tetrapositive Nickel as Alkali Nickel Periodate_NiPPI_Nature 1946.Pdf.
(31) Seo, H.; Cho, K. H.; Ha, H.; Park, S.; Hong, J. S.; Jin, K.; Nam, K. T. Water Oxidation Mechanism for 3d Transition Metal Oxide Catalysts under Neutral Condition. *J. Korean Ceram. Soc.* **2017**, *54* (1), 1–8. https://doi.org/10.4191/kcers.2017.54.1.12.
(32) Pan, G.; He, G.; Zhang, M.; Zhou, Q.; Tyliszczak, T.; Tai, R.; Guo, J.; Bi, L.; Wang, L.; Zhang, H. Nanobubbles at Hydrophilic Particle-Water Interfaces. *Langmuir* **2016**, *32* (43), 11133–11137. https://doi.org/10.1021/acs.langmuir.6b01483.
(33) Drevon, D.; Görlin, M.; Chernev, P.; Xi, L.; Dau, H.; Lange, K. M. Uncovering The Role of Oxygen in Ni-Fe(OxHy) Electrocatalysts Using In Situ Soft X-Ray Absorption Spectroscopy during the Oxygen Evolution Reaction. *Sci. Rep.* **2019**, *9* (1), 1532. https://doi.org/10.1038/s41598-018-37307-x.
(34) Walsh, A.; Watson, G. W.; Payne, D. J.; Edgell, R. G.; Guo, J.; Glans, P. A.; Learmonth, T.; Smith, K. E. Electronic Structure of the α and δ Phases of Bi2 O3: A Combined Ab Initio and x-Ray Spectroscopy Study. *Phys. Rev. B - Condens. Matter Mater. Phys.* **2006**, *73* (23), 1–13. https://doi.org/10.1103/PhysRevB.73.235104.
(35) de Groot, F. M. F.; Grioni, M.; Fuggle, J. C.; Ghijsen, J.; Sawatzky, G. A.; Petersen, H. Oxygen 1s X-Ray-Absorption Edges of Transition-Metal Oxides. *Phys. Rev. B* **1989**, *40* (8), 5715–5723. https://doi.org/10.1103/PhysRevB.40.5715.
(36) Gilbert, B.; Kim, C. S.; Dong, C. L.; Guo, J.; Nico, P. S.; Shuh, D. K. Oxygen K-Edge Emission and Absorption Spectroscopy of Iron Oxyhydroxide Nanoparticles. *AIP Conf. Proc.* **2007**, *882*, 721–725. https://doi.org/10.1063/1.2644643.
(37) Yoon, W. S.; Balasubramanian, M.; Chung, K. Y.; Yang, X. Q.; McBreen, J.; Grey, C. P.; Fischer, D. A. Investigation of the Charge Compensation Mechanism on the Electrochemically Li-Ion Deintercalated Li1-XCo1/3Ni1/3Mn 1/3O2 Electrode System by Combination of Soft and Hard X-Ray Absorption Spectroscopy. *J. Am. Chem. Soc.* **2005**, *127* (49), 17479–17487. https://doi.org/10.1021/ja0530568.
(38) Su, X.; Wang, Y.; Zhou, J.; Gu, S.; Li, J.; Zhang, S. Operando Spectroscopic Identification of Active Sites in NiFe Prussian Blue Analogues as Electrocatalysts: Activation of Oxygen Atoms for Oxygen Evolution Reaction. *J. Am. Chem. Soc.* **2018**, *140* (36), 11286–11292. https://doi.org/10.1021/jacs.8b05294.
(39) Isobe, H.; Shoji, M.; Shen, J.-R.; Yamaguchi, K. Chemical Equilibrium Models for the S3 State of the Oxygen-Evolving Complex of Photosystem II. *Inorg. Chem.* **2016**, *55* (2), 502–511. https://doi.org/10.1021/acs.inorgchem.5b02471.

(40) Li, X.; Siegbahn, P. E. M. Alternative Mechanisms for O2 Release and O–O Bond Formation in the Oxygen Evolving Complex of Photosystem II. *Phys. Chem. Chem. Phys.* **2015**, *17* (18), 12168–12174. https://doi.org/10.1039/C5CP00138B.
(41) Trotochaud, L.; Young, S. L.; Ranney, J. K.; Boettcher, S. W. Nickel-Iron Oxyhydroxide Oxygen-Evolution Electrocatalysts: The Role of Intentional and Incidental Iron Incorporation. *J. Am. Chem. Soc.* **2014**, *136* (18), 6744–6753. https://doi.org/10.1021/ja502379c.
(42) Enman, L. J.; Burke, M. S.; Batchellor, A. S.; Boettcher, S. W. Effects of Intentionally Incorporated Metal Cations on the Oxygen Evolution Electrocatalytic Activity of Nickel (Oxy)Hydroxide in Alkaline Media. *ACS Catal.* **2016**, *6* (4), 2416–2423. https://doi.org/10.1021/acscatal.5b02924.
(43) Hunter, B. M.; Winkler, J. R.; Gray, H. B. Iron Is the Active Site in Nickel/Iron Water Oxidation Electrocatalysts. *Molecules* **2018**, *23* (4). https://doi.org/10.3390/molecules23040903.

TOC Graphic for manuscript